Supplementary material

Abstract

This document presents the supplementary material for the paper: X. Zhou, S. Leonardos, X. Hu, and K. Daniilidis. 3D Shape Estimation from 2D Landmarks: A Convex Relaxation Approach. In CVPR, 2015.

1. Proof of Proposition 1

Proof. Since $\mathcal{S} = \{\boldsymbol{Y} \mid \boldsymbol{Y} = s\boldsymbol{X}, \boldsymbol{X} \in \mathcal{Q}\}$, we have

$$\begin{aligned} \text{conv}(\mathcal{S}) &= \left\{ \sum_{i=1}^{k} \theta_i \boldsymbol{Y}_i \middle| \ \boldsymbol{Y}_i \in \mathcal{S}, \theta_i \geq 0, \sum_{i=1}^{k} \theta = 1 \right\} \\ &= \left\{ \sum_{i=1}^{k} \theta_i (s\boldsymbol{X}_i) \middle| \ \boldsymbol{X}_i \in \mathcal{Q}, \theta_i \geq 0, \sum_{i=1}^{k} \theta = 1 \right\} \\ &= s \cdot \text{conv}(\mathcal{Q}). \end{aligned}$$

□

2. Algorithm to solve Problem (12)

The problem can be rewritten as:

$$\begin{aligned} \min_{\widetilde{\boldsymbol{M}}, \boldsymbol{Z}} \ & \sum_{i=1}^{k} \|\boldsymbol{M}_i\|_2, \\ \text{s.t.} \ \ & \boldsymbol{W} = \boldsymbol{Z}\widetilde{\boldsymbol{B}}, \\ & \widetilde{\boldsymbol{M}} = \boldsymbol{Z}. \end{aligned} \tag{1}$$

The augmented Lagrangian is

$$\begin{aligned} \mathcal{L}_\mu \left(\widetilde{\boldsymbol{M}}, \boldsymbol{Z}, \boldsymbol{Y}\right) = & \sum_{i=1}^{k} \|\boldsymbol{M}_i\|_2 + \left\langle \boldsymbol{Y}, \widetilde{\boldsymbol{M}} - \boldsymbol{Z} \right\rangle \\ & + \frac{\mu}{2} \left\| \widetilde{\boldsymbol{M}} - \boldsymbol{Z} \right\|_F^2, \\ \text{s.t.} \ \ & \boldsymbol{W} = \boldsymbol{Z}\widetilde{\boldsymbol{B}} \end{aligned} \tag{2}$$

Then, the steps in (3) to (5) are iterated to update variables:

$$\widetilde{\boldsymbol{M}}^{t+1} = \arg\min_{\widetilde{\boldsymbol{M}}} \mathcal{L}_\mu \left(\widetilde{\boldsymbol{M}}, \boldsymbol{Z}^t, \boldsymbol{Y}^t\right); \tag{3}$$

$$\boldsymbol{Z}^{t+1} = \arg\min_{\boldsymbol{Z}} \mathcal{L}_\mu \left(\widetilde{\boldsymbol{M}}^{t+1}, \boldsymbol{Z}, \boldsymbol{Y}^t\right); \tag{4}$$

$$\boldsymbol{Y}^{t+1} = \boldsymbol{Y}^k + \mu \left(\widetilde{\boldsymbol{M}}^{t+1} - \boldsymbol{Z}^{t+1}\right). \tag{5}$$

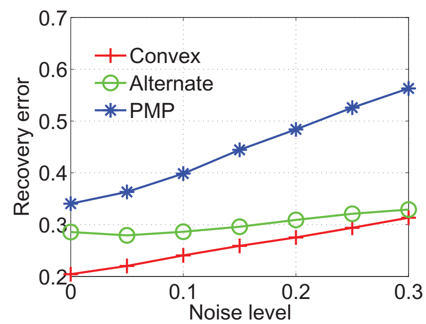

Figure 1. The mean reconstruction error for human poses with simulated Gaussian noise.

The only modification is the Z-step since minimizing $\mathcal{L}_\mu \left(\widetilde{\boldsymbol{M}}, \boldsymbol{Z}, \boldsymbol{Y}\right)$ over $\boldsymbol{Z}$ in (2) is solving an equality-constrained quadratic programming problem, which admits the following closed-form solution:

$$\boldsymbol{Z}^{t+1} = \boldsymbol{Z}^0 + \left(\widetilde{\boldsymbol{M}}^{t+1} + \boldsymbol{Y}^k - \boldsymbol{Z}^0\right) \boldsymbol{N}\boldsymbol{N}^T, \tag{6}$$

where $\boldsymbol{Z}^0$ is a particular solution to $\boldsymbol{W} = \boldsymbol{Z}\widetilde{\boldsymbol{B}}$ and $\boldsymbol{N}$ denotes the left null space of $\widetilde{\boldsymbol{B}}$.

3. Sensitivity to noise

We add simulated Gaussian noise to the Mocap dataset (subject 15) to evaluate the algorithms in noisy cases. The plot of reconstruction error versus the noise level is given in Figure 1.

4. Basis shapes for cars

Figure 2 shows the basis shapes for car shape estimation in Section 5.2.2 in the paper.

5. Face estimation

We simply demonstrate the applicability of the proposed method for 3D face reconstruction using the FaceWarehouse [1]. We use the blendshapes provided in the dataset as the basis shapes, fit the shape model to the annotated landmarks in the image, and finally reconstruct the 3D shape with the estimated shape parameters and the meshes of blendshapes. Some examples are shown in Figure 3.

978-1-4673-6964-0/15/$31.00 ©2015 IEEE

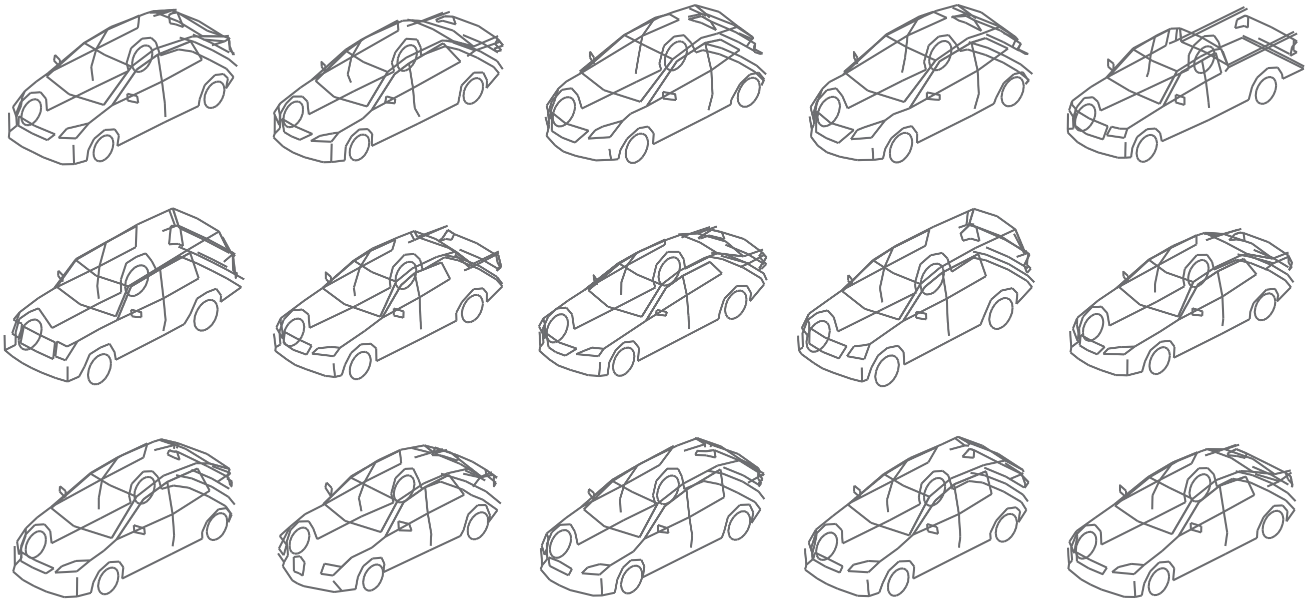

Figure 2. Basis shapes for cars.

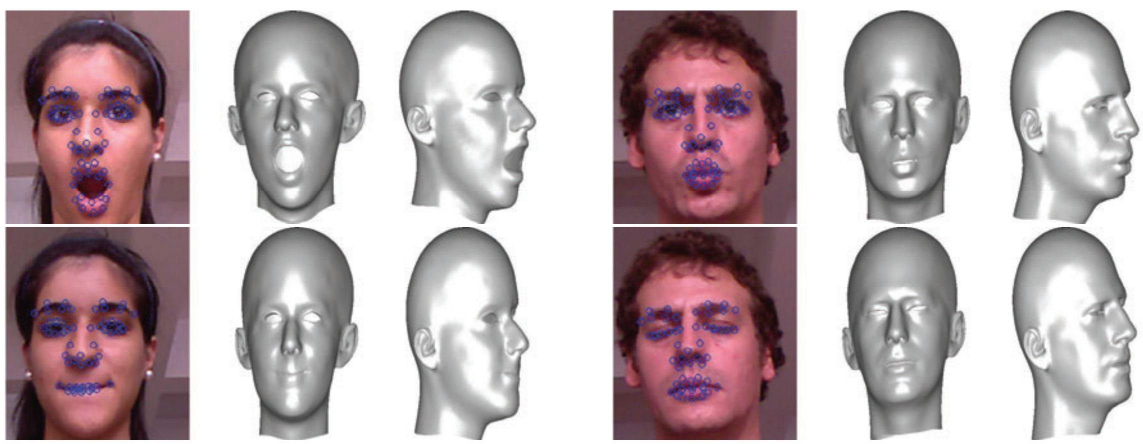

Figure 3. Examples of face reconstruction. For each example, the landmarks superposed on the image and the reconstructed faces from two views are displayed.

References

[1] C. Cao, Y. Weng, S. Zhou, Y. Tong, and K. Zhou. Facewarehouse: A 3d facial expression database for visual computing. *IEEE Transactions on Visualization and Computer Graphics*, 20(3):413–425, 2014. 1